3-21-2023

Prominent Size Effects without a Depolarization Field Observed in Ultrathin Ferroelectric Oxide Membranes

Haoying Sun

Jiahui Gu

Yongqiang Li

Tula R. Paudel

Di Liu

See next page for additional authors

Authors

Haoying Sun, Jiahui Gu, Yongqiang Li, Tula R. Paudel, Di Liu, Jierong Wang, Yipeng Zang, Chengyi Gu, Jiangfeng Yang, Wenjie Sun, Zhengbin Gu, Evgeny Y. Tsymbal, Junming Liu, Houbing Huang, Di Wu, and Yuefeng Nie

Prominent Size Effects without a Depolarization Field Observed in Ultrathin Ferroelectric Oxide Membranes

Haoying Sun[1,2] Jiahui Gu[1,2] Yongqiang Li[3,4] Tula R. Paudel[5,6] Di Liu[7] Jierong Wang[1,2]
Yipeng Zang[1,2,8] Chengyi Gu[1,2] Jiangfeng Yang[1,2] Wenjie Sun[1,2] Zhengbin Gu[1,2] Evgeny Y. Tsymbal[5,9]
Junming Liu[3] Houbing Huang[7] Di Wu[1,2,*] and Yuefeng Nie[1,2,†]

[1]*National Laboratory of Solid State Microstructures, Jiangsu Key Laboratory of Artificial Functional Materials,*
College of Engineering and Applied Sciences, Nanjing University, Nanjing 210093, China
[2]*Collaborative Innovation Center of Advanced Microstructures, Nanjing University, Nanjing 210093, China*
[3]*National Laboratory of Solid State Microstructures and Department of Physics,*
Collaborative Innovation Center of Advanced Microstructures, Nanjing University, Nanjing 210093, China
[4]*State Key Laboratory of Laser Interaction with Matter, Northwest Institute of Nuclear Technology, Xi'an, Shaanxi 710024, China*
[5]*Department of Physics and Astronomy, University of Nebraska–Lincoln, Lincoln, Nebraska 68583, USA*
[6]*Department of Physics, South Dakota School of Mines and Technology, Rapid City, South Dakota 57701, USA*
[7]*Advanced Research Institute of Multidisciplinary Science, Beijing Institute of Technology, Beijing 100081, China*
[8]*School of Materials Science and Engineering, Anhui University, Hefei 230601, China*
[9]*Nebraska Center for Materials and Nanoscience, University of Nebraska–Lincoln, Lincoln, Nebraska 68588, USA*

The increasing miniaturization of electronics requires a better understanding of material properties at the nanoscale. Many studies have shown that there is a ferroelectric size limit in oxides, below which the ferroelectricity will be strongly suppressed due to the depolarization field, and whether such a limit still exists in the absence of the depolarization field remains unclear. Here, by applying uniaxial strain, we obtain pure in-plane polarized ferroelectricity in ultrathin $SrTiO_3$ membranes, providing a clean system with high tunability to explore ferroelectric size effects especially the thickness-dependent ferroelectric instability with no depolarization field. Surprisingly, the domain size, ferroelectric transition temperature, and critical strain for room-temperature ferroelectricity all exhibit significant thickness dependence. These results indicate that the stability of ferroelectricity is suppressed (enhanced) by increasing the surface or bulk ratio (strain), which can be explained by considering the thickness-dependent dipole-dipole interactions within the transverse Ising model. Our study provides new insights into ferroelectric size effects and sheds light on the applications of ferroelectric thin films in nanoelectronics.

Ferroelectric oxides with ABO_3 perovskite structures, exhibiting multitudinous robust performances in high dielectric permittivities [1–3] and piezoelectric responses [4–7], have promoted promising electronic applications such as nonvolatile ferroelectric memories [8–12], piezoelectric sensors [6], capacitors [13,14], and energy harvesters [15]. The ever-increasing commercial demands for high-density integration and portability of electronics further provide growing impetus to seek stable ferroelectricity at low dimensions. However, the ferroelectricity in oxides is strongly dependent on film thickness. Suffering from pronounced size effects, the ferroelectricity can be suppressed or even ruined when film thickness shrinks down to the nanoscale [16–25]. A remarkable challenge, as a result, is to disclose the key mechanism of size effects in perovskite ferroelectrics for optimizing the practical design of devices.

To date, many studies on ferroelectric size effects have been attempted both theoretically and experimentally [17–20,23–35]. Early reports have shown that the size effects of ferroelectricity require a critical volume, approximately hundreds of nanometers, to align the electric dipoles [27,30]. Nevertheless, with the rapid development in fabrication techniques over the past decades, much smaller critical thickness values (a few nanometers) have been demonstrated in high-quality ferroelectric films [16–22], providing an abundant opportunity for exploring intrinsic size effects. On the grounds of these experimental discoveries and in light of the specific electrical boundary condition of imperfect screening at surfaces, the theory of depolarization field [31–34,36] is developed to account for observed size effects in ultrathin ferroelectrics, especially for out-of-plane polarized perovskite oxides such as $BaTiO_3$ [16–18] and $PbTiO_3$ [20–22]. However, in regard to the case without a depolarization field, a systematic investigation is largely absent, whereas it is still nontrivial whether size effects will exist and how the ferroelectric properties evolve with thickness in this situation. As the Mermin-Wagner theorem dictates that the long-range magnetic order is strongly suppressed by thermal fluctuations in ultrathin ferromagnetic materials [37], whether such an

inherent dimensionality effect exists in ferroelectric materials regardless of the depolarization field remains elusive. Some theoretical calculations [38–40] regarding this problem have been presented to enlighten these explorations, but direct experimental confirmation remains insufficient. Benefiting from the recently developed film transfer and stretch methods [5,41–45], purely in-plane ferroelectricity with a ferroelectric transition temperature (T_c) up to 400 K has been realized in freestanding SrTiO$_3$ (STO) membranes [42], providing a clean and unique platform for studying the possible unconventional size effects unrelated to the depolarization field.

In this Letter, we synthesize freestanding STO membranes with various thicknesses and investigate their thickness-dependent stability of ferroelectricity under uniaxial tensile strain. At reduced thickness, ultrathin in-plane polarized STO membranes exhibit suppressed T_c, enhanced critical strain for room-temperature ferroelectricity, and reduced domain size. All these results suggest the presence of a pronounced ferroelectric size effect even without a depolarization field, which can be explained by considering thickness-dependent dipole-dipole interactions within the framework of the transverse Ising model.

A series of STO films with a thickness of n unit cell (u.c.) ($n = 5, 7, 10, 15, 20$) were grown on single-crystalline (001) STO substrates with Sr$_3$Al$_2$O$_6$ sacrificial buffer layers by molecular beam epitaxy, as described elsewhere

5,46,47]]. The experimental film transfer and the stretching process are sketched in Supplemental Material, Fig. S1 [48]. Typical reflection high-energy electron diffraction (RHEED) intensity oscillations and high-resolution x-ray diffraction (XRD) scans both indicate the high quality of epitaxial STO films (Fig. S2 [48]). By transferring STO membranes onto flexible substrates (polyethylene naphihalate, PEN) using the thermosetting glue of epoxy, atomically smooth surfaces with clear step terraces can be well preserved on the lateral millimeter scale (Fig. S1 [48]). Moreover, the possible extrinsic morphology effects on ferroelectricity can be ruled out. After transfer, the stretching force (denoted as **F**) is exerted onto the PEN to apply continuously tunable tensile strain along the [100] direction. According to the first-principles density functional theory calculations in Fig. S3 and Ref. [48], in-plane ferroelectricity of the STO membrane emerges in the stretched sample, and the value of polarization enhances with the increased uniaxial tensile strain. The actual strain state of STO membranes is calibrated using XRD, with a measurement error of $\pm 0.04\%$ (Fig. S4 [48]). To investigate the dynamics of in-plane ferroelectricity under the precisely controlled strains, an *in situ* homemade device for strain engineering is designed. As schematized in Fig. 1(a), this device is compatible with both XRD and scanning probe microscopy (SPM) characterizations.
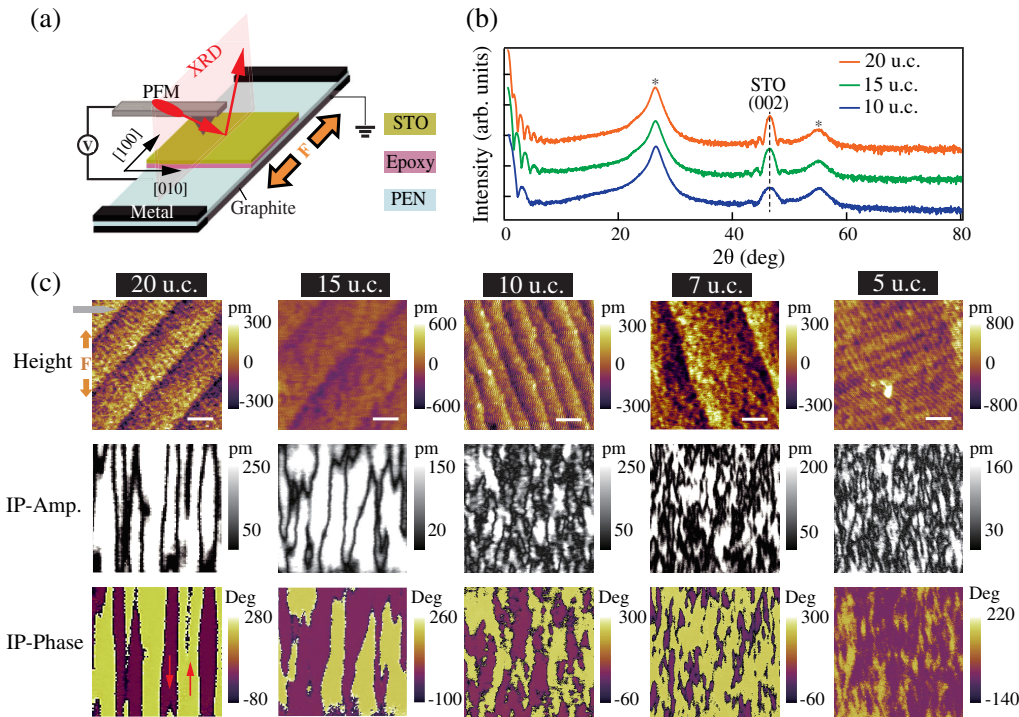

FIG. 1. Thickness-dependent domain structures under a fixed strain of 1.8%. (a) Schematic of the device for strain engineering. The STO membranes are attached to a polymer substrate (PEN) using epoxy. The cantilever is placed with its arm perpendicular to the stretching direction to detect the in-plane polarization along the [100] direction. (b) High-resolution XRD $2\theta - \omega$ scans for 10–20 u.c. thick STO/epoxy/PEN samples. Asterisks denote the PEN diffraction peaks; the vertical dotted line marks the position of the STO (002) diffraction peak. (c) LPFM height, amplitude, and phase images (from top to bottom) for STO membranes with various thicknesses. Red arrows denote the polarization orientations. The scale bars are 400 nm.

First, the crystal quality of unstrained freestanding STO membranes is examined by XRD. In Fig. 1(b), clear thickness fringes and Kiessig fringes are observed for 10, 15, and 20 u.c. STO membranes, indicating the well-preserved single crystallinity as well as a macroscopically large-area flat surface. For example, in Fig. S2(b) [48], the overall roughness and thickness are found to be 240 pm and 6 nm, respectively, in a 15 u.c. STO membrane, similar to the pristine states of as-grown films. Note that diffraction intensities for 5 and 7 u.c. STO membranes are too weak to be detected here. The local morphology and ferroelectric order are probed using SPM methods. Specifically, lateral piezoresponse force microscopy (LPFM) is used for high-resolution visualization of the in-plane domain structures. No response is observed in both the out-of-plane and in-plane PFM signals from as-grown STO films as well as unstrained STO membranes, consistent with its quantum paraelectric nature.

Having established that in-plane ferroelectricity can be induced by uniaxial strain, we next investigate thickness-dependent ferroelectric behaviors of STO membranes by varying the film thickness while keeping other parameters identical, especially the uniaxial strain. When increasing tensile strain to a large value of 1.8%, all transferred STO membranes demonstrate robust room-temperature ferroelectricity. As shown in Fig. 1(c) and Fig. S5 [48], stripe-textured in-plane 180° multidomains and switchable piezo-hysteresis loops are observed in LPFM measurements, among which the strain-induced 180° stripe domain in thick STO membranes is consistent with the recent work by Xu *et al.* [42]. The formation of such stripe domains is most likely related to nucleation process of ferroelectric domains. Under uniaxial strain, there are two equivalent antiparallel ferroelectric polarizations. As the ferroelectric stability increases, ferroelectric nucleation starts from any place and finally evolves into stripe domains. The specific in-plane polarization orientation of such domains, along [100] or [$\bar{1}$00] is determined by trailing field methods [62,63]. Temperature-dependent LPFM measurements indicate that the domain size and morphology do not vary with the thermal history (Fig. S6 [48]). During the whole stretching process, no out-of-plane ferroelectric signal is observed, while the in-plane polarization responses are gradually enhanced along with the increasing uniaxial strain. Moreover, the in-plane domain configurations are strongly thickness dependent. Under the identical tensile strain of 1.8%, the domain structure in 5 u.c. $SrTiO_3$ is quite distinct from that in 15 u.c. $SrTiO_3$: the domain sizes are smaller, and domain density is higher [Fig. 1(c)].

To quantitatively analyze the thickness-dependent domain structures, the corresponding average domain sizes and domain areas for multiple samples, including but not limited to Fig. 1(c), are calculated for repeated validations. And the data were taken in large and uniform areas inside the samples to avoid the possible impact of defects and nonuniform strain near the sample edge. Figure 2 shows
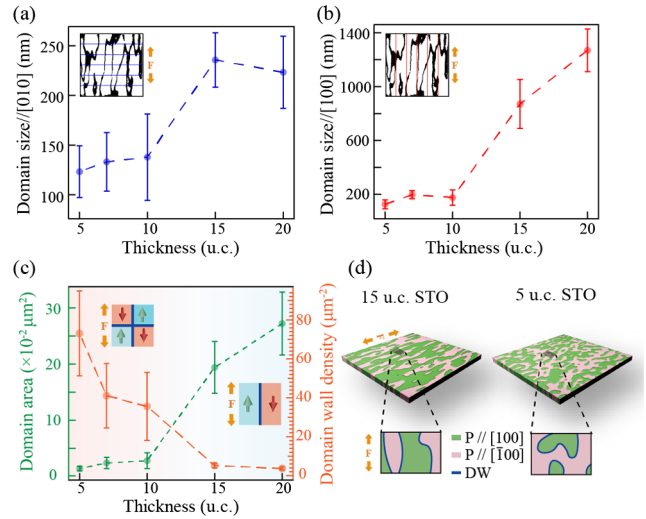

FIG. 2. Quantitative analysis and phase-field simulations. Average domain sizes along the [010] (a) and the [100] (b) directions illustrating strong dependence on the film thickness. Insets display the corresponding positions of five linecuts to count the number of domains for meaningful statistics. (c) Average domain area as a function of film thickness. Insets: Two types of domain configurations. (d) Phase-field simulations of domain patterns from 15 and 5 u.c. STO membranes with a strain of 1.8%, respectively. Domain wall (DW); error bars represent the standard deviations.

that both of the sizes and areas evolve dramatically over the thickness range tested. For the domain size statistics, five linecuts with equal spacing are performed in the binarized amplitude patterns parallel and perpendicular to the stretching direction, as shown in the insets of Figs. 2(b) and 2(b). A detailed demonstration to extract average domain size is illustrated in Fig. S7 [48]. By counting the number of domain walls (minima) that cross these line profiles, the numbers of parallel and vertical domains can be obtained accordingly. The average domain area for each film is calculated as the product of the parallel and vertical domain sizes. Quantified data are shown in Figs. 2(a)–2(c), which suggests that the domain size decreases not only along the [100] direction but also along the [010] direction with reduced thickness. Correspondingly, the domain area is also scaled down. These results are consistent with the phase-field simulation results, showing that 5 u.c. STO membranes display relatively smaller domain size and higher domain wall density than 15 u.c membranes at the same strain of 1.8% [Fig. 2(d)]. The shrunken domain size at reduced thickness is most likely related to the lower T_c and weaker polarization in ultrathin membranes. And similar dependences of domain size on polarization and T_c have been reported previously in the cases of out-of-plane ferroelectrics [24,64–66]. These similarities imply that the shrunken domain size is most likely related to the lower ferroelectric instability, but a full understanding of these observations requires further investigations. It is

noteworthy that the narrower domain size brings about higher domain wall density in 5–10 u.c. STO membranes [Fig. 1(c)]. One interesting aspect of this evolution of domain configuration is the formation of high-density charged domain walls [67,68], the head-to-head and tail-to-tail 180° domain walls, as depicted in the insets of Fig. 2(c) and Fig. S1 [48].

Apart from the evolution of domain structures, we also explored the evolution of the ferroelectric Curie temperature, T_c, as a function of thickness. The dielectric measurements show a significant shift of T_c with increasing strain as shown in Figs. 3(a) and S8. Note that the broad transition observed in our strained STO membranes may indicate the possible relaxorlike ferroelectric behavior, similar to the features previously reported in epitaxially strained titanate films [69–71]. These T_c values show a nearly linear dependence on the uniaxial strain [Fig. 3(c)],
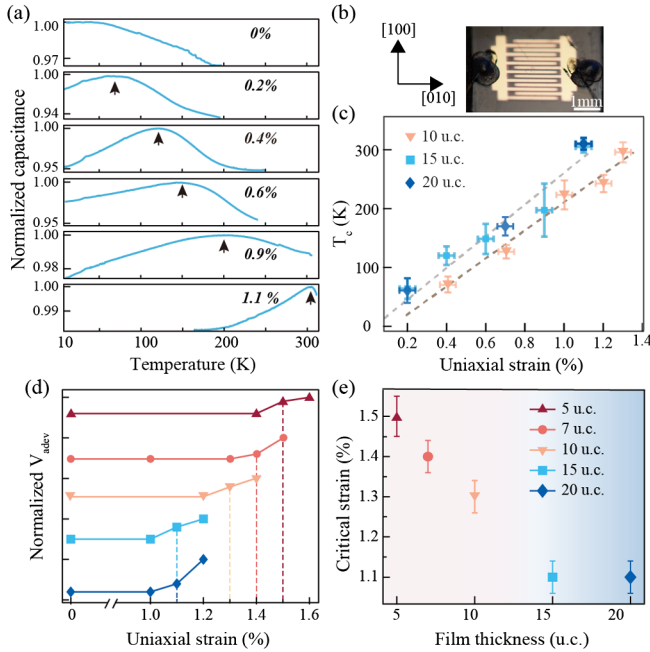
similar to previous reports [3,42], indicating the possibility of using strain to predict T_c and vice versa. As we define the critical strain in a way that room-temperature ferroelectricity occurs, the experimental criterion for identifying the emergence of room-temperature ferroelectricity and the critical strain is a noticeable transition in LPFM amplitude and phase images. For example, the determination of a critical strain of 10 u.c. STO membrane is demonstrated in Fig. S9 [48]. From the strain-induced variation in LPFM amplitude intensity, we extract the average deviation (V_{adev}) of intensity profiles integrated over the [100] axis, along which the domain grows and propagates. As shown in Fig. 3(d), for every STO membrane with different thicknesses, the steep upturns in the V_{adev} vs strain curves signify the emergence of room-temperature T_c.

Figure 3(e) summarizes the behavior of critical strain as a function of film thickness. Every critical strain value was repeatedly verified using samples of different batches with the same thickness. In addition, the critical strain values for 10, 15, and 20 u.c. STO membranes extracted from the dielectric capacitance peaks in Fig. 3(c), are the same as those determined from the LPFM results in Fig. 3(d). Obviously, at the same strain state, the ferroelectric transition temperature decreases as the film thickness decreases, further providing strong evidence for the presence of ferroelectric size effects. The observed abnormal increase in the critical strain at 10 u.c. or thinner STO membranes [Fig. 3(e)] is in line with the transition in domain configurations [Fig. 1(c)]. Both of them corroborate the prominent size effects in in-plane polarized STO membranes.

We now turn to discuss the origin of ferroelectric size effects in strained STO membranes. With a zero depolarization field, the suppression of ferroelectricity in thinner membranes is most likely associated with the increasing surface-to-volume ratio and the different chemical boundary conditions at the surface, the two main factors emphasized in the transverse Ising model [49,50,72–79]. This model is used to microscopically describe the ferroelectric transition by considering thickness-dependent dipole-dipole interactions within the framework of the pseudospin theory, which has been commonly employed to describe the phase transition in STO [80–82]. By considering of the nearest-neighbor interactions, the Hamiltonian of the system is written as (for details see the Supplemental Material [48])

$$H = -\Omega_i \sum_i S_i^x - \frac{1}{2} \sum_{i,j} J_{ij} S_i^z S_j^z,$$

where S_i^x and S_i^z are the x and z components of a pseudospin operator at site i and J_{ij} is the interaction between the i_{th} and j_{th} sites, with i and j running over all sites. The transverse field Ω determines the rate of tunneling of Ti atom from one potential minima to the other in the double-well energy landscape. It is an energy perturbation term related to thermal hopping [30], which

FIG. 3. Thickness-dependent T_c of strained STO membranes. (a) Dielectric characterizations revealing strain-tunable T_c in a 15 u.c. STO/epoxy/PEN sample. Considering the relatively broader peaks of the measured curves, the first derivative of capacitance was used to extract the peak positions (black arrows). (b) Optical image of coplanar interdigital electrodes deposited on the surface of the 15 u.c. STO membrane. (c) The extracted T_c values of 10–20 u.c. STO as a function of uniaxial strain. Error bars include the uncertainty of peak positions extracted from multiple measurements (vertical) and errors in measuring strain (horizontal). (d) Normalized average deviation (V_{adev}) of amplitude intensity vs uniaxial strain revealing domain formation at room temperature. Curves for various thicknesses are offset for clarity. The vertical dashed lines indicate the position of critical strain for room-temperature ferroelectricity. (e) Thickness-dependent critical strain for stretched STO membranes. Error bars come from the measurement error of strain.

tends to disorder the parallel alignment of pseudospins through quantum tunneling across the two double-well ground states, while the J_{ij} favors ordered alignment of dipoles. As a result, a phase transition occurs when the disorder effects are comparable with the ordered effects, which is sensitive to the strain and thickness of the STO membranes in our case.

Generally, due to the fewer nearest neighboring sites at the surface, as schematized in Fig. 4(a), the overall surface dipole-dipole interaction is naturally weaker than bulk interaction. Therefore, as the thickness scales down, the surface-to-volume ratio is elevated, and weak surface dipole-dipole interactions dominate the overall polarization state. The stability of ferroelectricity of the membrane is thus impaired and even ruined below a critical thickness. Accompanied with this, it results in the lower T_c. The surface J_s is typically weaker than bulk J in many materials [83–86], which will further strengthen the descending trend of T_c with reduced thickness. Likewise, the dipole (polarization) orientation at the surface layer is more susceptible
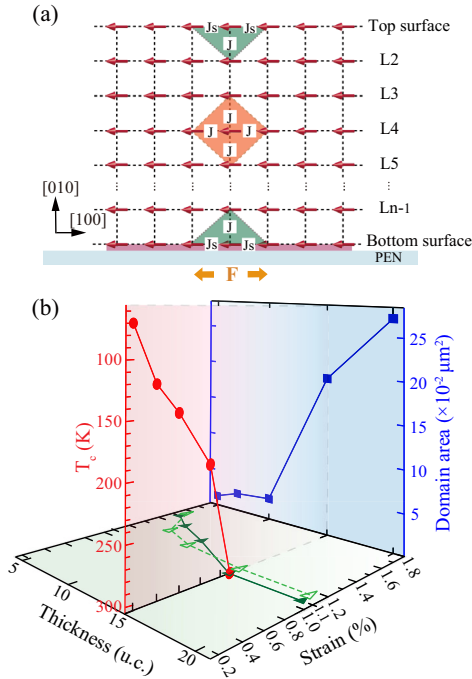

FIG. 4. The origin of the ferroelectric size effects. (a) Schematic illustration of the dipole-dipole interaction in a transverse Ising model considering nearest-neighbor interactions. J_s is the surface dipole-dipole interaction strength, while J is the bulk dipole-dipole interaction strength. The green triangle and orange box represent the nearest-neighbor interactions at the surface and in the bulk, respectively. (b) Summarized phase diagram of STO membranes unveiling how ferroelectricity (domain area and T_c) evolves with film thickness and uniaxial strain. Solid lines represent the experimental results, while the green dashed line is the simulated data obtained from the transverse Ising model (see Fig. S10). Different scales are used in the strain axis for clarification.

to thermal vibration. Consequently, in our experiment, lower T_c (larger critical strain) and smaller domain sizes are observed in thinner membranes ($n \leq 10$ u.c.). Larger critical strain values are required to produce sufficient atomic displacements (enhanced J_s and J) to stabilize ferroelectricity in thinner membranes and reach the same transition temperature as thick ones.

To gain more insight into how the film thickness affects T_c, the theory of the transverse Ising model is adopted to simulate the relationship of critical strain vs thickness by only taking the nearest neighboring dipole-dipole interaction into account, as shown in Fig. S10 [48]. With this simple toy model, the simulated results show a tendency consistent with our experimental observations, manifesting a gradual upsurge in the critical strain at a reduced scale. Furthermore, the ratio between surface J_s and bulk J can be deduced to be approximately 0.8 for the best agreement between simulations and experimental data, implying the suppressed dipole-dipole exchange strength at the surface than in the bulk. As a result, for STO membranes, the weak surface dipole-dipole interaction can be ascribed to the fewer nearest neighboring sites as well as weaker J_s. Detailed simulation information can be found in the Supplemental Material [48].

For the sake of intuitively imaging thickness-dependent size effects of in-plane ferroelectric STO membranes, the corresponding domain area and T_c as functions of film thickness and uniaxial strain are summarized and plotted in Fig. 4(b), indicating the close correlation between these parameters. Specifically, we observed prominent in-plane ferroelectric size effects in uniaxially strained ultrathin STO membranes, revealing that size effects still exist in ferroelectrics even without a depolarization field. The significant suppression in domain size (area) and transition temperature T_c is established in thinner STO membranes (5–10 u.c.). Such progressive destabilization of ferroelectricity can be explained via the transverse Ising model from thickness-dependent dipole-dipole interactions. Although we simplified the transverse Ising model by neglecting the difference in J between parallel and perpendicular polarizations and the role of the next-nearest neighbor, this simple toy model still captures the key physics and reflects the expected trend. If such factors are considered, it is believed that the simulation should have a better match with experiments. Note that while we mainly use the transverse Ising model to provide a simple explanation of the experimental observations, a full understanding of the underlying mechanisms requires in-depth theoretical investigations using various modes, such as the soft mode theory [72,87,88].

It is also important to note that the dipole-dipole interaction we discussed in STO membranes does not merely exist in purely in-plane ferroelectrics, instead, in all ferroelectrics. As expected, for out-of-plane ferroelectrics, the depolarization field-effect combined with the

thickness-dependent dipole-dipole interaction should be considered to explain the observed size effects. Similar to the dimensionality effects on long-range magnetic ordering, our observations inply that such effects also exist in ferroelectric materials regardless of the depolarization field. Also note that our results show that even in the thinnest films (5 u.c.), room-temperature ferroelectricity exists, which indicates that the critical thickness may be absent in these systems as long as the dipole-dipole interaction is strong enough. This encouraging prediction offers tantalizing prospects for nanoelectronic devices. Last, the presence of high-density domain walls observed at reduced thickness brings new opportunities for the artificial creation of high-density conductive domain walls in ultrathin ferroelectric membranes, offering a promising avenue for nonvolatile memory devices through dimensionality engineering. With this ideal in-plane polarized ferroelectric membrane system, we show the inherent size effects of ferroelectricity driven by thickness-dependent dipole-dipole interactions and their high tunability by applying uniaxial strain. Therefore, our study inspires new insights into ferroelectric size effects and provides instructive design for ferroelectric devices.

---

[*]diwu@nju.edu.cn

[†]ynie@nju.edu.cn

[1] M. T. Buscaglia, M. Viviani, V. Buscaglia, L. Mitoseriu, A. Testino, P. Nanni, Z. Zhao, M. Nygren, C. Harnagea, D. Piazza et al., High dielectric constant and frozen macroscopic polarization in dense nanocrystalline BaTiO$_3$ ceramics, Phys. Rev. B **73**, 064114 (2006).

[2] A. R. Damodaran, E. Breckenfeld, Z. Chen, S. Lee, and L. W. Martin, Enhancement of ferroelectric Curie temperature in BaTiO$_3$ films via strain-induced defect dipole alignment, Adv. Mater. **26**, 6341 (2014).

[3] J. H. Haeni, P. Irvin, W. Chang, R. Uecker, P. Reiche, Y. L. Li, S. Choudhury, W. Tian, M. E. Hawley, B. Craigo et al., Room-temperature ferroelectricity in strained SrTiO$_3$, Nature (London) **430**, 758 (2004).

[4] Z. Guan, H. Hu, X. W. Shen, P. H. Xiang, N. Zhong, J. H. Chu, and C. G. Duan, Recent progress in two-dimensional ferroelectric materials, Adv. Electron. Mater. **6**, 1900818 (2020).

[5] D. Ji, S. Cai, T. R. Paudel, H. Sun, C. Zhang, L. Han, Y. Wei, Y. Zang, M. Gu, Y. Zhang et al., Freestanding crystalline oxide perovskites down to the monolayer limit, Nature (London) **570**, 87 (2019).

[6] J. F. Scott, Applications of modern ferroelectrics, Science **315**, 954 (2007).

[7] L. Zhang, J. Chen, L. Fan, O. Dieguez, J. Cao, Z. Pan, Y. Wang, J. Wang, M. Kim, S. Deng et al., Giant polarization in super-tetragonal thin films through interphase strain, Science **361**, 494 (2018).

[8] J. F. Scott and C. A. Paz de Araujo, Ferroelectric memories, Science **246**, 1400 (1989).

[9] O. Auciello, J. F. Scott, and R. Ramesh, The physics of ferroelectric memories, Phys. Today **51**, No. 7, 22 (1998).

[10] R. Waser and A. Rudiger, Pushing towards the digital storage limit, Nat. Mater. **3**, 81 (2004).

[11] Z. Wen, C. Li, D. Wu, A. Li, and N. Ming, Ferroelectric-field-effect-enhanced electroresistance in metal/ferroelectric/semiconductor tunnel junctions, Nat. Mater. **12**, 617 (2013).

[12] Z. Wen and D. Wu, Ferroelectric tunnel junctions: Modulations on the potential barrier, Adv. Mater. **32**, e1904123 (2020).

[13] J. Y. Jo, Y. S. Kim, T. W. Noh, J. G. Yoon, and T. K. Song, Coercive fields in ultrathin BaTiO$_3$ capacitors, Appl. Phys. Lett. **89**, 232909 (2006).

[14] C. J. G. Meyers, C. R. Freeze, S. Stemmer, and R. A. York, (Ba, Sr)TiO$_3$ tunable capacitors with RF commutation quality factors exceeding 6000, Appl. Phys. Lett. **109**, 112902 (2016).

[15] T. Y. Kim, S. K. Kim, and S. W. Kim, Application of ferroelectric materials for improving output power of energy harvesters, Nano Converg. **5**, 30 (2018).

[16] D. A. Tenne, P. Turner, J. D. Schmidt, M. Biegalski, and S. K. Streiffer, Ferroelectricity in Ultrathin BaTiO$_3$ Films: Probing the Size Effect by Ultraviolet Raman Spectroscopy, Phys. Rev. Lett. **103**, 177601 (2009).

[17] Y. S. Kim, D. H. Kim, J. D. Kim, Y. J. Chang, T. W. Noh, J. H. Kong, K. Char, Y. D. Park, S. D. Bu, J. G. Yoon et al., Critical thickness of ultrathin ferroelectric BaTiO$_3$ films, Appl. Phys. Lett. **86**, 506 (2005).

[18] D. J. Kim, J. Y. Jo, Y. S. Kim, Y. J. Chang, J. S. Lee, J. G. Yoon, T. K. Song, and T. W. Noh, Polarization Relaxation Induced by a Depolarization Field in Ultrathin Ferroelectric Capacitors, Phys. Rev. Lett. **95**, 237602 (2005).

[19] P. Maksymovych, M. Huijben, M. Pan, S. Jesse, N. Balke, Y.-H. Chu, H. J. Chang, A. Y. Borisevich, A. P. Baddorf, G. Rijnders, D. H. A. Blank, R. Ramesh, and S. V. Kalinin, Ultrathin limit and dead-layer effects in local polarization switching of BiFeO$_3$, Phys. Rev. B **85**, 014119 (2012).

[20] C. Lichtensteiger, J. M. Triscone, J. Junquera, and P. Ghosez, Ferroelectricity and Tetragonality in Ultrathin PbTiO$_3$ Films, Phys. Rev. Lett. **94**, 047603 (2005).

[21] R. Takahashi, O. Dahl, E. Eberg, J. K. Grepstad, and T. Tybell, Ferroelectric stripe domains in PbTiO$_3$ thin films: Depolarization field and domain randomness, J. Appl. Phys. **104**, 064109 (2008).

[22] D. D. Fong, A. M. Kolpak, J. A. Eastman, S. K. Streiffer, P. H. Fuoss, G. B. Stephenson, C. Thompson, D. M. Kim,

K. J. Choi, C. B. Eom *et al.*, Stabilization of Monodomain Polarization in Ultrathin PbTiO$_3$ Films, Phys. Rev. Lett. **96,** 127601 (2006).

[23] P. Gao, Z. Zhang, M. Li, R. Ishikawa, B. Feng, H. J. Liu, Y. L. Huang, N. Shibata, X. Ma, S. Chen *et al.*, Possible absence of critical thickness and size effect in ultrathin perovskite ferroelectric films, Nat. Commun. **8,** 15549 (2017).

[24] D. D. Fong, G. B. Stephenson, S. K. Streiffer, J. A. Eastman, O. Auciello, P. H. Fuoss, and C. Thompson, Ferroelectricity in ultrathin perovskite films, Science **304,** 1650 (2004).

[25] V. Nagarajan, S. Prasertchoung, T. Zhao, H. Zheng, J. Ouyang, R. Ramesh, W. Tian, X. Q. Pan, D. M. Kim, C. B. Eom *et al.*, Size effects in ultrathin epitaxial ferroelectric heterostructures, Appl. Phys. Lett. **84,** 5225 (2004).

[26] K. A. Rabe, M. Dawber, C. Lichtensteiger, C. H. Ahn, and J. M. Triscone, *Physics of Ferroelectrics: A Modern Perspective* (Springer, Berlin, 2007), ISBN 978-3-540-34591-6.

[27] T. M. Shaw, S. Trolier-McKinstry, and P. C. McIntyre, The properties of ferroelectric films at small dimensions, Annu. Rev. Mater. Sci. **30,** 263 (2000).

[28] D. R. Tilley and B. Zeks, Landau theory of phase-transitions in thick-films, Solid State Commun. **49,** 823 (1984).

[29] C. L. Wang and S. R. P. Smith, Landau theory of the size-driven phase-transition in ferroelectrics, J. Phys. Condens. Matter **7,** 7163 (1995).

[30] M. E. Lines and A. M. Glass, *Principles and Applications of Ferroelectrics and Related Materials* (Clarendon Press, Oxford, 1977).

[31] I. P. Batra and B. Silverman, Thermodynamic stability of thin ferroelectric films, Solid State Commun. **11,** 291 (1972).

[32] R. R. Mehta, B. D. Silverman, and J. T. Jacobs, Depolarization fields in thin ferroelectric films, J. Appl. Phys. **44,** 3379 (1973).

[33] I. P. Batra, P. Wurfel, and B. D. Silverman, Phase-transition, stability, and depolarization field in ferroelectric thin-films, Phys. Rev. B **8,** 3257 (1973).

[34] J. Junquera and P. Ghosez, Critical thickness for ferroelectricity in perovskite ultrathin films, Nature (London) **422,** 506 (2003).

[35] G. Pacchioni and S. Valeri, *Oxide Ultrathin Films: Science and Technology* (Wiley-VCH Verlag GmbH & Co. KGaA, New York, 2012), Chap. 12, ISBN 978-3-527-64017-1.

[36] D. Zhao, T. Lenz, G. H. Gelinck, P. Groen, D. Damjanovic, D. M. de Leeuw, and I. Katsouras, Depolarization of multi-domain ferroelectric materials, Nat. Commun. **10,** 2547 (2019).

[37] N. D. Mermin and H. Wagner, Absence of Ferromagnetism or Antiferromagnetism in One- or Two-Dimensional Isotropic Heisenberg Models, Phys. Rev. Lett. **17,** 1133 (1966).

[38] Henu Sharma, Jens Kreisel, and Philippe Ghosez, First-principles study of PbTiO$_3$ under uniaxial strains, and stresses, Phys. Rev. B **90,** 214102 (2014).

[39] G. Geneste, E. Bousquet, and P. Ghosez, New insight into the concept of ferroelectric correlation volume, J. Comput. Theor. Nanosci. **5,** 517 (2008).

[40] Turan Birol, Nicole A. Benedek, and Craig J. Fennie, Interface Control of Emergent Ferroic Order in Ruddlesden-Popper Sr$_{n+1}$Ti$_n$O$_{3n+1}$, Phys. Rev. Lett. **107,** 257602 (2011).

[41] L. Di, D. J. Baek, S. S. Hong, L. F. Kourkoutis, Y. Hikita, and H. Y. Hwang, Synthesis of freestanding single-crystal perovskite films and heterostructures by etching of sacrificial water-solublelayers, Nat. Mater. **15,** 1255 (2016).

[42] R. Xu, J. Huang, E. S. Barnard, S. S. Hong, P. Singh, E. K. Wong, T. Jansen, V. Harbola, J. Xiao, B. Y. Wang *et al.*, Strain-induced room-temperature ferroelectricity in SrTiO$_3$ membranes, Nat. Commun. **11,** 3141 (2020).

[43] S. S. Hong, M. Gu, M. Verma, V. Harbola, B. Y. Wang, D. Lu, A. Vailionis, Y. Hikita, R. Pentcheva, J. M. Rondinelli *et al.*, Extreme tensile strain states in La$_{0.7}$Ca$_{0.3}$MnO$_3$ membranes, Science **368,** 71 (2020).

[44] S. S. Hong, J. H. Yu, D. Lu, A. F. Marshall, Y. Hikita, Y. Cui, and H. Y. Hwang, Two-dimensional limit of crystalline order in perovskite membrane films, Sci. Adv. **3,** eaao5173 (2017).

[45] G. Dong, S. Li, M. Yao, Z. Zhou, Y. Q. Zhang, X. Han, Z. Luo, J. Yao, B. Peng, Z. Hu *et al.*, Super-elastic ferroelectric single-crystal membrane with continuous electric dipole rotation, Science **366,** 475 (2019).

[46] H. Y. Sun, Z. W. Mao, T. W. Zhang, L. Han, T. T. Zhang, X. B. Cai, X. Guo, Y. F. Li, Y. P. Zang, W. Guo *et al.*, Chemically specific termination control of oxide interfaces via layer-by-layer mean inner potential engineering, Nat. Commun. **9,** 2965 (2018).

[47] H. Y. Sun, C. C. Zhang, J. M. Song, J. H. Gu, T. W. Zhang, Y. P. Zang, Y. F. Li, Z. B. Gu, P. Wang, and Y. F. Nie, Epitaxial optimization of atomically smooth Sr$_3$Al$_2$O$_6$ for freestanding perovskite films by molecular beam epitaxy, Thin Solid Films **697,** 137815 (2020).

[48] See Supplemental Material at http://link.aps.org/supplemental/10.1103/PhysRevLett.130.126801 for experimental methods and additional results of film transfer and characterization, LPFM measurements, first-principles calculations, phase-field simulations, dielectric measurements, and calculations of T_c via the transverse Ising model (Figs. S1–S10), which includes Refs. [42,49–61].

[49] C. L. Wang, W. L. Zhong, and P. L. Zhang, The Curie-temperature of ultra-thin ferroelectric films, J. Phys. Condens. Matter **4,** 4743 (1992).

[50] C. L. Wang, S. R. P. Smith, and D. R. Tilley, Ferroelectric thin-film described by an Ising-model in a transverse field, J. Phys. Condens. Matter **6,** 9633 (1994).

[51] P. E. Blochl, Projector augmented-wave method, Phys. Rev. B **50,** 17953 (1994).

[52] J. P. Perdew and A. Zunger, Self-interaction correction to density-functional approximations for many-body systems, Phys. Rev. B **23,** 5048 (1981).

[53] G. G. Kresse and J. J. Furthmüller, Efficient iterative schemes for Ab initio total-energy calculations using a plane-wave basis set, Phys. Rev. B **54,** 11169 (1996).

[54] G. Kresse and D. Joubert, From ultrasoft pseudopotentials to the projector augmented-wave method, Phys. Rev. B **59,** 1758 (1999).

[55] H. J. Monkhorst and J. D. Pack, Special points for Brillouin-zone integrations, Phys. Rev. B **13,** 5188 (1976).

[56] N. A. Pertsev, A. K. Tagantsev, and N. Setter, Phase transitions and strain-induced ferroelectricity in $SrTiO_3$ epitaxial thin films, Phys. Rev. B **61**, R825 (2000).

[57] D. Liu, R. Zhao, H. M. Jafri, J. Wang, and H. Huang, Phase-field simulations of surface charge-induced polarization switching, Appl. Phys. Lett. **114**, 112903 (2019).

[58] Y. L. Li, S. Choudhury, J. H. Haeni, M. D. Biegalski, A. Vasudevarao, A. Sharan, H. Z. Ma, J. Levy, V. Gopalan, and S. Trolier-McKinstry *et al.*, Phase transitions and domain structures in strained pseudocubic (100) $SrTiO_3$ thin films, Phys. Rev. B **73**, 184112 (2006).

[59] G. Sheng, Y. L. Li, J. X. Zhang, S. Choudhury, Q. X. Jia, V. Gopalan, D. G. Schlom, Z. K. Liu, and L. Q. Chen, Phase transitions and domain stabilities in biaxially strained (001) $SrTiO_3$ epitaxial thin films, J. Appl. Phys. **108**, 3593 (2010).

[60] C. L. Wang, S. R. P. Smith, and D. R. Tilley, Ferroelectric thin films described by an Ising model in a transverse field, J. Phys. Condens. Matter **6**, 9633 (1994).

[61] M. G. Cottam, D. R. Tilley, and B. Zeks, Theory of surface modes in ferroelectrics, J. Phys. C **17**, 1793 (1984).

[62] S. Matzen, O. Nesterov, G. Rispens, J. A. Heuver, M. Biegalski, H. M. Christen, and B. Noheda, Super switching and control of in-plane ferroelectric nanodomains in strained thin films, Nat. Commun. **5**, 4415 (2014).

[63] R. K. Vasudevan, Y. Matsumoto, X. Cheng, A. Imai, S. Maruyama, H. L. Xin, M. B. Okatan, S. Jesse, S. V. Kalinin, and V. Nagarajan, Deterministic arbitrary switching of polarization in a ferroelectric thin film, Nat. Commun. **5**, 4971 (2014).

[64] Y. G. Wang, W. L. Zhong, and P. L. Zhang, Surface and size effects on ferroelectric films with domain structures, Phys. Rev. B **51**, 5311 (1995).

[65] S. K. Streiffer, J. A. Eastman, D. D. Fong, C. Thompson, A. Munkholm, M. V. Ramana Murty, O. Auciello, G. R. Bai, and G. B. Stephenson, Observation of Nanoscale 180° Stripe Domains in Ferroelectric $PbTiO_3$ Thin Films, Phys. Rev. Lett. **89**, 067601 (2002).

[66] G. B. Stephenson and K. R. Elder, Theory for equilibrium 180° stripe domains in $PbTiO_3$ films, J. Appl. Phys. **100**, 051601 (2006).

[67] J. Ma, J. Ma, Q. Zhang, R. Peng, J. Wang, C. Liu, M. Wang, N. Li, M. Chen, X. Cheng *et al.*, Controllable conductive readout in self-assembled, topologically confined ferroelectric domain walls, Nat. Nanotechnol. **13**, 947 (2018).

[68] P. Sharma, Q. Zhang, D. Sando, C. H. Lei, Y. Liu, J. Li, V. Nagarajan, and J. Seidel, Nonvolatile ferroelectric domain wall memory, Sci. Adv. **3**, e1700512 (2017).

[69] H. W. Jang, A. Kumar, S. Denev, M. D. Biegalski, P. Maksymovych, C. W. Bark, C. T. Nelson, C. M. Folkman, S. H. Baek, N. Balke *et al.*, Ferroelectricity in Strain-Free $SrTiO_3$ Thin Films, Phys. Rev. Lett. **104**, 197601 (2010).

[70] M. D. Biegalski, Y. Jia, D. G. Schlom, S. Trolier-McKinstry, S. K. Streiffer, V. Sherman, R. Uecker, and P. Reiche, Relaxor ferroelectricity in strained epitaxial $SrTiO_3$ thin films on $DyScO_3$ substrates, Appl. Phys. Lett. **88**, 192907 (2006).

[71] C. H. Lee, N. D. Orloff, T. Birol, Y. Zhu, V. Goian, E. Rocas, R. Haislmaier, E. Vlahos, J. A. Mundy, L. F. Kourkoutis *et al.*, Exploiting dimensionality and defect mitigation to create tunable microwave dielectrics, Nature (London) **502**, 532 (2013).

[72] R. Blinc and B. Žekš, *Soft Modes in Ferroelectrics and Antiferroelectrics* (North-Holland, Amsterdam, 1974).

[73] P. Gennes, Collective motions of hydrogen bonds, Solid State Commun. **1**, 132 (1963).

[74] C. L. Wang and S. R. P. Smith, Dynamics of ferroelectric thin films described by the transverse Ising model, J. Phys. Condens. Matter **8**, 3075 (1996).

[75] Y. G. Wang, W. L. Zhong, and P. L. Zhang, Ferroelectric films described by transverse Ising model with long-range interactions, Solid State Commun. **101**, 807 (1997).

[76] P. N. Sun, T. Q. Lu, H. Chen, and W. W. Cao, Polarization properties of ferroelectric thin films on transverse Ising model, Phys. Status Solidi (b) **245**, 2599 (2008).

[77] A. Oubelkacem, I. Essaoudi, A. Ainane, M. Saber, J. Gonzalez, and K. Bärner, Ferroelectric films described by the transverse Ising model, Physica (Amsterdam) **404B**, 4190 (2009).

[78] F. C. Sa Barreto, Ferroelectric phase transitions, and the Ising model, Braz. J. Phys. **30**, 779 (2000).

[79] C. L. Wang, Y. Xin, X. S. Wang, and W. L. Zhong, Size effects of ferroelectric particles described by the transverse Ising model, Phys. Rev. B **62**, 11423 (2000).

[80] J. Hemberger, M. Nicklas, R. Viana, P. Lunkenheimer, A. Loidl, and R. Böhmer, Quantum paraelectric and induced ferroelectric states in $SrTiO_3$, J. Phys. Condens. Matter **8**, 4673 (1996).

[81] J. Hemberger, P. Lunkenheimer, R. Viana, R. Böhmer, and A. Loidl, Electric-field-dependent dielectric constant and nonlinear susceptibility in $SrTiO_3$, Phys. Rev. B **52**, 13159 (1995).

[82] K. S. Chapman and W. A. Atkinson, Modified transverse Ising model for the dielectric properties of $SrTiO_3$ films and interfaces, J. Phys. Condens. Matter **32**, 065303 (2020).

[83] A. G. Zembilgotov, N. A. Pertsev, H. Kohlstedt, and R. Waser, Ultrathin epitaxial ferroelectric films grown on compressive substrates: Competition between the surface and strain effects, J. Appl. Phys. **91**, 2247 (2002).

[84] R. Kretschmer and K. Binder, Surface effects on phase-transitions in ferroelectrics and dipolar magnets, Phys. Rev. B **20**, 1065 (1979).

[85] W. L. Zhong, Y. G. Wang, P. L. Zhang, and B. D. Qu, Phenomenological study of the size effect on phase transitions in ferroelectric particles, Phys. Rev. B **50**, 698 (1994).

[86] Y. Su, H. Chen, J. J. Li, A. K. Soh, and G. J. Weng, Effects of surface tension on the size-dependent ferroelectric characteristics of free-standing $BaTiO_3$ nano-thin films, J. Appl. Phys. **110**, 084108 (2011).

[87] W. Cochran, Crystal stability and the theory of ferroelectricity, Adv. Phys. **9**, 387 (1960).

[88] P. Ghosez and J. Junquera. First-principles modeling of ferroelectric oxide nanostructures, *Handbook of Theoretical & Computational Nanotechnology* (American Scientific Publisher, Stevenson Ranch CA, USA, 2006), Chap. 134.